

Cavitation in Electron Fluids and the Puzzles of Photoemission Spectra in Alkali Metals

Roman Dmitriev

Department of Chemistry, University of Houston, Houston, TX 77204-5003

Jenny Green

*St. John's School, Houston, TX 77019**

Vassiliy Lubchenko[†]

Department of Chemistry, University of Houston, Houston, TX 77204-5003

Department of Physics, University of Houston, Houston, TX 77204-5005 and

Texas Center for Superconductivity,

University of Houston, Houston, TX 77204-5002

(Dated: February 1, 2024)

Abstract

Angle-resolved photoemission spectra of alkali metals exhibit a puzzling, non-dispersing peak in the apparent density of states near the Fermi energy. We argue that the holes left behind a significant fraction of photoejected electrons are not wavepacket-like objects used to describe excitations of an equilibrium Fermi liquid but, instead, are relatively localized entities resulting from a photon-induced cavitation in the electron fluid. At the same time, these special localized holes can be thought of as vacancies in a transient Wigner solid. The corresponding contribution to the photoemission current is non-dispersive and is tied to the Fermi level; it exhibits certain similarities to photoemission from localized core orbitals such as the presence of recoil currents. Calculated spectra are consistent with experiment. We briefly discuss the present findings in the context of quantum measurement.

Angle-resolved spectra of sodium and potassium exhibit a distinct, peculiar peak near the Fermi energy, within a substantial range of photon energies.^{1–3} This peak does not move with the photon’s energy and is narrower than the momentum-conserving, dispersing peak. The intensity of the non-dispersing peak is substantial even when the initial state of the electron for a *vertical* transition would be above the Fermi energy. Furthermore in potassium, it is the dispersing peak that is often hard to resolve,² while the anomalous peak is clearly visible. The Fermi surfaces in Na and K are particularly simple—nearly spherical in fact—and fully contained within the first Brillouin zone;⁴ thus no sharp features in the density of states are expected. Surface states do not seem to be at play either, since the resulting peaks, if any, would not be strictly tied to the Fermi energy.

Mahan and coworkers^{5,6} argued that the peculiar photoemission peak is a wing of the dispersing peak when the latter is centered at electron energies above the Fermi surface; the broadening is due to interactions and their interplay with the free surface. Detailed estimates^{5,6} yield photoemission spectra that are qualitatively similar to some of those observed in sodium for photon energies corresponding to the $(1, 1, 0) \rightarrow (3, 3, 0)$ transitions, but lack the anomalous “balcony peaks” seen in the adjacent range of photon energies that correspond to the $(1, 1, 0) \rightarrow (-4, -4, 0)$ transitions.⁷ The situation with potassium is even less conclusive.⁸

Overhauser⁹ proposed, alternatively, that the anomalous peak results from a static charge density wave (CDW).¹⁰ Sodium does become close-packed at sufficiently low temperatures thus implying, potentially, a structural instability. Still, experimental studies¹¹ decisively rule out the presence of a static CDW, consistent with recent studies¹² according to which the Fermi surface of sodium is relatively insensitive to the detailed structure of the crystal. A detailed review of previous work can be found in Ref.³

Here we argue that the puzzling photoemission peak is caused by non-adiabatic effects that are not amenable to perturbative expansions around the equilibrium state of the electron assembly. The frequency ω_{ph} of the incoming photon is much greater than the typical rates of electronic motions, $\omega_{\text{ph}} \gg v_F/a$, where v_F and a are the Fermi velocity and lattice spacing, respectively. Thus one expects a response similar to giant resonances seen in nuclear spectra,¹³ though spanning a relatively narrow spectral range because the plasma oscillations are in their ground state at the energies in question. To quantify the photocurrent one must compute the one-particle density function $\rho(\mathbf{r}_1, \mathbf{r}_2)$ of the electron.

The momentum-like argument \mathbf{k} of the Wigner transform of the latter density matrix, $\rho(\mathbf{r}, \mathbf{k}) = \int d^3(\mathbf{r}_2 - \mathbf{r}_1) \rho(\mathbf{r}_1, \mathbf{r}_2) e^{-i\mathbf{k}(\mathbf{r}_2 - \mathbf{r}_1)}$, essentially corresponds to the momentum \mathbf{k} of the electronic wavepacket, while the dependence of the latter Wigner transform on the center-of-mass variable $\mathbf{r} = (\mathbf{r}_1 + \mathbf{r}_2)/2$ reflects the spatial variation of the corresponding charge density. Landau's Fermi-liquid theory corresponds to the limit of this spatial variation being very slow and describes the quasi-equilibrium response of the electron fluid.¹⁴ Conversely, high-frequency motions of the electron fluid, $\omega > v_F/a$, are heavily hybridized with the plasmons via Landau damping,^{15,16} whereby the charge density varies on length scales comparable to the lattice spacing. This, then, suggests a possibility that in addition to extended electron wavepackets characteristic of the equilibrium, Fermi-liquid behavior, the fast photons can also knock out individual electrons in the form of localized entities.

In fact, just this latter possibility is the only one that could be realized classically. For concreteness, we consider a setup in which a compact region of a Newtonian fluid changes its velocity instantaneously from zero to v_0 , as it would in response to a sudden perturbation applied to the region. Specifically for a spherically-shaped region of radius R , the reactive force of the surrounding fluid depends on time in the following manner, per the solved problem 24.9 from Ref.¹⁷:

$$F(t) = 6\pi\eta Rv_0 \left[1 + R\sqrt{\rho/t\pi\eta} \right] + \frac{2\pi}{3}\rho R^3 v_0 \delta(t) \quad (1)$$

where η and ρ are the viscosity and density, respectively, of the fluid. The intensity of dissipation is given by $v_0 F(t)$. Of interest here is the non-adiabatic contribution $\propto t^{-1/2}$ to the viscous part of the response, which represents a characteristic hydrodynamic tail and, tellingly, scales with the area of the sphere. The corresponding loss spectrum amounts to an inverse-square root peak $\omega^{-1/2}$, which diverges at low energies. The latter low energies would correspond to the vicinity of the Fermi energy in an electron fluid.

This notion prompts us to inquire whether a classical-like photoemission from localized electronic states can occur—as a bulk phenomenon—in quantum fluids made of electrons. It would suffice for such localization, if any, to be only transient, because of the short duration of photoemission events. Localization of particles in the bulk simply means the particles have formed a solid. A solid is a state of broken translational symmetry in which the particles are each assigned to specific sites in space; the particles perform vibrational motions around their respective sites.¹⁸ The notion of a solid-like component to the wavefunction of an

electron fluid may seem surprising, at first. We recall however that the electric current, if any, is exclusively due to the electrons' ability to tunnel through classically forbidden, inter-nuclear regions. One may associate the time spent in classically-forbidden regions with the liquid component of the wavefunction. The remaining time electrons perform bound motions within the classically allowed regions, each region assigned to a corner of a lattice. These motions correspond to a solid-like component of the overall wave function and lower translational symmetry, even if transiently.

Let us construct the solid-like component for a monovalent solid, which houses one electron per site. Begin with a Wigner solid of the jellium, whereby the electrons are sufficiently far apart and the positive charge is uniformly distributed.¹³ Imagine a process where we uniformly compress the system. To compensate for the concomitant increase in the kinetic energy of the electrons, we redistribute the positive charge so as to create a local excess of positive charge at the lattice sites of the original Wigner solid; the sites will become the actual atomic nuclei at the end of the compression process. (The number of sites remains constant during the process. The pertinent Wigner solid does not have to be strictly periodic,¹⁹ thus allowing for vibrational displacements of the nuclei and a variety of cell shapes.) Since the barriers in the crystal field that separate distinct lattice sites are finite, a fluid component to the electronic wavefunction will appear eventually. Because the number of electrons per site remains constant, the “compression construct” represents a continuous process; thus the solid-like and the liquid-like components of the electron assembly coexist, when both are present. The two phases remain in mutual equilibrium, while their respective mole fractions depend on the extent of the compression. This effective coexistence of two distinct phase behaviors in the very same region of space is analogous to what happens during the crossover to activated transport in liquids,^{18,20} when metastable structures begin to form. Translational symmetry is broken on times scales shorter than the lifetimes of the metastable structures but is restored on longer times. Note a co-existence of liquid and solid behaviors, respectively, has been reported for Hartree-Fock solutions in jellium.²¹

Within a single-electron picture, the localized states can be thought of as bound states individual electrons transiently create for each other on short times. (This is in addition to the potentials due to the ionic cores, of course). The corresponding energy levels are, however, not well-defined because the electrons are not static. The resulting line broadening is analogous to what happens during spectral diffusion,^{22,23} since the leading contribution

of local charge fluctuation to the shift of on-site energies is dipole-dipole, owing to charge conservation. An electron moves from site to site at rate v_F/a , while inducing a local dipole moment change ea . These effective dipoles are uniformly distributed at concentration $n \sim 1/a^3$. Contributions of individual dipoles to the overall spectral shift are roughly $\sim (ae)^2/r^3 \equiv A/r^3$ each fluctuating at rate $\gamma \sim v_F/a$. The width of the corresponding spectral line increases with time^{22,23} at the rate $\sim nA\gamma = (e^2/a)(v_F/a) \simeq E_F(v_F/a)$. The broadening on the time scale π/ω_{ph} of a photoemission event is, then, roughly $E_F(v_F/a\omega_{\text{ph}}) \sim 10^{-1}E_F$, consistent with experiment. The solid-like response will be progressively diminished for slower experimental probes, the overall response ultimately approaching that of a Fermi liquid.

The liquid-like and solid-like contributions to the wavefunction correspond to two distinct, non-overlapping components of the overall wavefunction characterized by pronounced localization in the momentum and direct space, respectively. Indeed, already the ground state of an electron fluid in the presence of a scattering potential is orthogonal to the ground state in the absence of the potential.²⁴ Very generally, a solid must be separated by a discontinuous transition from the fluid state.^{18,25,26} Consequently, the two phases occupy disconnected portions of the phase space. Because of this lack of overlap between the liquid-like and solid-like contributions to the overall wavefunction, we may present the total intensity of the photocurrent as a weighted sum of the respective intensities of those two contributions:

$$I(E) = x_{\text{liq}}I_{\text{liq}}(E) + x_{\text{sol}}I_{\text{sol}}(E), \quad (2)$$

where E is the energy of the detected electron and $x_{\text{liq}} + x_{\text{sol}} = 1$, by construction.

To estimate the solid-like contribution $I_{\text{sol}}(E)$ to the photocurrent, we first note that in the spectral range in question¹⁻³ no plasmons are produced. Indeed, the plasmon frequency in Na, 5.7 eV,²⁷ is significantly greater than the Fermi energy, 2.8 eV.¹ In other words, our transient electron solid recoils as a whole. We will approximate this solid as harmonic. The coordinates of any lattice fragments thus obey the Gaussian distribution;²⁸ denote the corresponding variance with δr^2 . The probability for the solid to recoil as a whole, after the fragment absorbs or emits momentum q , is given by $e^{-q^2(\delta r)^2}$, a notion used in Mössbauer spectroscopy.²⁹ Conversely, the expression $e^{-q^2(\delta r)^2}$ can be viewed, up to a multiplicative factor, as the probability distribution for a local harmonic degree of freedom δr that is compatible with a zero-phonon recoil of the lattice at momentum q . The corresponding

ground state wave function is $\psi_q(\mathbf{r}) = (q^2/\pi)^{3/4} e^{-q^2 r^2/2}$, where q represents a parameter. We thus estimate the photocurrent $I_{\text{sol}}(E)$, due to localized initial states, by first evaluating the current using the function $\psi_q(\mathbf{r})$ as the initial state, for a given value of q , and then averaging over a pertinent distribution of q . The set of recoil values q , due to emitting a localized electron, should be consistent with the rate of spatial variation of the valence electrons. At values k_f of the momentum of the outgoing electron pertinent to Plummer et al.'s experiment, $k_f \sim 3k_F$, the valence wave function can be largely approximated by the frontier atomic orbital ψ_{fr} on an individual center. (For Na, this would be the 3s orbital.) Thus we use the magnitude squared of the normalized Fourier transform $|\tilde{\psi}_{\text{fr}}(q)|^2$, times $4\pi q^2$, as the probability distribution for the parameter q .

The (zero-plasmon) recoil due to the transient-solid component of the electron assembly causes a negligibly small shift of the photoemission spectrum, as does the recoil due to the pertinent nuclei. If it were not for the recoil due to the electron fluid, localized electrons would be all extracted near the Fermi energy, the latter nominally corresponding to a quiescent fluid devoid of currents, consistent with the classical limit considered above. This notion can be also formulated quantum-mechanically, in an effective single-electron picture: Single-particle states for the extended and localized states tend to mutually repel,^{30,31} while the extended states form a continuous band. Our effective localized states—which note are not tied to lone pairs, impurity levels, or surface states etc.—are thus “pushed” outside of the continuous band. At the same time, there should be no gap between the delocalized and localized states either, because the two sets of states correspond, respectively, to a liquid and solid that co-exist, as already mentioned. Consequently, the chemical potentials of the phases are mutually equal, which pegs the emission line for localized electrons near the Fermi energy of the electron liquid. Conversely, no such matching of the chemical potentials is expected in non-monovalent metals, because there is no continuous process that converts a Wigner solid into a lattice with more than one electron per site. The resulting mismatch in the chemical potentials actually corresponds to the recoil energy of the electrons sharing the site with the photoejected electron. Thus we predict that in non-monovalent metals, there will *also* be a photocurrent due to localized sources, but the energy of the outgoing electron will be down shifted, relative to the Fermi level, by the said recoil energy.

The dispersing part of the photocurrent is, likewise, largely determined by the Fourier transform of the wavefunction of the atomic valence shell, but within a near vicinity of

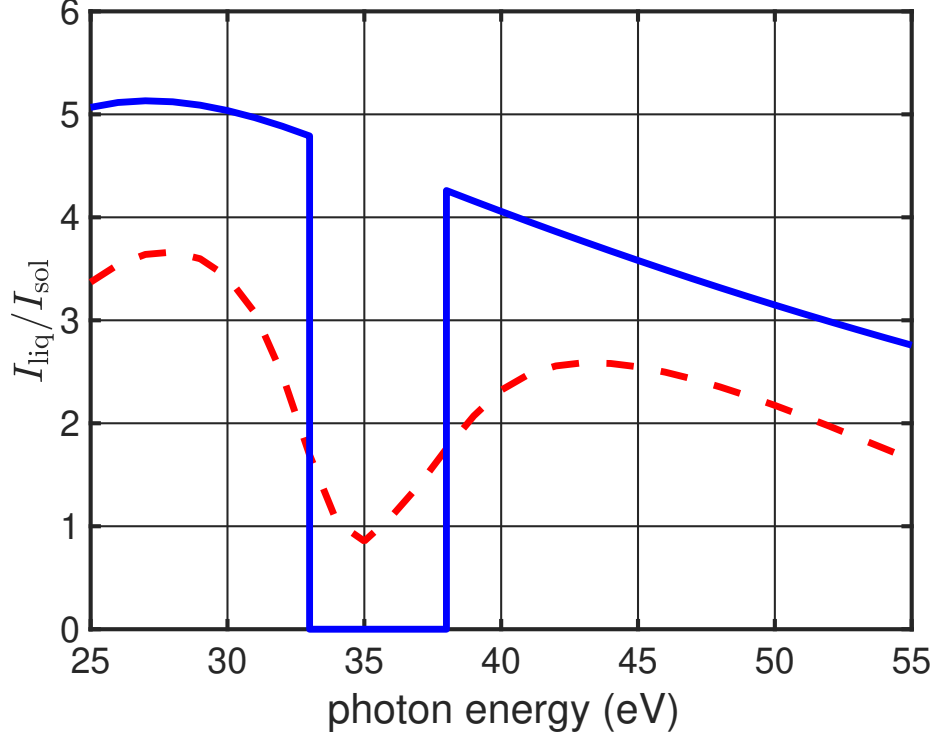


FIG. 1. The ratio of the integrated photocurrents from Eq. (3) as a function of the photon frequency without (solid line) and with (dashed line) line broadening effects included.

the momentum of the outgoing electron, according to a standard calculation^{32–39} detailed in Supplemental Material.⁴⁰ When the broadening of the dispersing peak is neglected, one obtains a rather simple expression for the relative intensity of the liquid- and solid-like contributions to the photocurrent, at a given value of the photon frequency:

$$\frac{I_{\text{liq}}}{I_{\text{sol}}} = \frac{\pi^{1/2}}{2} \frac{k_{f,\text{liq}}^3}{k_{f,\text{sol}}^3} \frac{\left| \tilde{\psi}_{\text{fr}}(k_{f,\text{liq}}) \right|^2}{\int_0^\infty \frac{dq}{q} e^{-k_{f,\text{sol}}^2/q^2} \left| \tilde{\psi}_{\text{fr}}(q) \right|^2}. \quad (3)$$

Here $k_{f,\text{liq}}$ and $k_{f,\text{sol}}$ denote the momentum for the outgoing electron extracted as a wave-packet and localized object, respectively. The two momenta are rather close numerically because the photon frequency is much greater than E_F . According to Eq. (3), the contribution of the localized electrons is distributed over a broad momentum range and, thus, should be suppressed but only several-fold relative to the momentum-conserving transitions, except when the latter transitions fall into the spectrally forbidden region. The result of the calculation, shown in Fig. 1 with the solid line, is consistent with this expectation.

The peak due to localized sources of photocurrent is intrinsically broadened owing to the

short-lived nature of the effective confining potential due to the transient electronic solid, as already discussed. Smaller in magnitude, but significant methodologically is the broadening of the Fermi-energy peak due to recoil currents of the electron fluid. These currents must arise because a spatially uniform fluid is not the ground state of the electron assembly in the presence of a bounding potential due to the (photo-induced) localized hole. The recoil currents are entirely analogous to those arising during photoemission from a deep localized state. Under the latter circumstances, a sharp absorption line will broaden to become a skewed peak, the low-energy side of which is an integrable power divergence.^{41,42}

$$I_{\text{sol}}(E) \propto \frac{1}{(E - E_f)^{1-\alpha}} \quad (4)$$

where

$$\alpha = 2 \sum_l (2l + 1)(\delta_l/\pi)^2 \quad (5)$$

and δ_l is the phase shift for scattering, due to the aforementioned local potential, at value l of the angular momentum. As alluded to already, the majority of scattering in alkali metals occurs at $l = 0$. If we assume, for simplicity, that the scattering is exclusively in the $l = 0$ channel and that the Friedel sum rule⁴³ $1 = (2/\pi) \sum_l (2l + 1)\delta_l$ applies, we obtain $\delta_0 = \pi/2$, thus yielding $\alpha = 1/2$. This is the same exponent for the loss spectrum as in the classical limit of the Newtonian liquid considered earlier. Consistent with this notion, the phase shift $\pi/2$ corresponds to a purely viscous response, whereby for an oscillating signal $e^{i\omega t}$ the momentum transfer rate goes as $\eta(d/dt)e^{i\omega t} = \eta\omega e^{i(\omega t + \pi/2)}$. Still, one should generally expect scattering at $l > 0$ as well, which will amount to deviations from the hydrodynamic result in Eq. (1).

Although the localized electron is extracted near the absorption edge, the present situation is distinct from the X-ray edge problem. There, the excited electron (hole) scatters from a core orbital right into the continuum perturbed by the excess local potential created by the excitation; thus the electron (hole) itself contributes to the recoil currents and, in turn, the overall response of the fluid.^{42,44} Here, instead, the outgoing electron—which had been localized in the first place—does not itself contribute to the recoil currents. Thus in contrast with the conventional edge problem, the recoil always results in a divergence at the spectrum's edge.

We estimate the weights x_{liq} and x_{sol} in Eq. (2) by comparing the times valence electrons

spend in classically forbidden and allowed regions, respectively

$$\frac{x_{\text{liq}}}{x_{\text{sol}}} \approx 4D \frac{t_{\text{forbidden}}}{t_{\text{allowed}}}. \quad (6)$$

where we have also included the transmission coefficient D for the tunneling so as to account only for successful tunneling attempts. Because the occupied portion of the valence band in alkali metals is comparable in width to that of a free electron gas at the same density, one may assume that the potential energy barrier separating two nearest neighbor sites is sufficiently narrow so that the shape of the potential energy maximum separating two nearest-neighbor ionic cores can be well approximated by an inverted parabola. Thus the time the electron travels one way under the barrier is given by $t_{\text{forbidden}} = \pi/\omega^\ddagger$, where ω^\ddagger is the frequency of the motion within the parabola. We estimate the frequency ω^\ddagger by using the curvature of the Thomas-Fermi potential at distances corresponding to the midpoint between two nearest atoms in the lattice. The residence time in the classical region is determined by the plasmon frequency itself, $t_{\text{allowed}} = \pi/\omega_p$, since this is the pertinent frequency for charge oscillations even on small lengthscales $\sim a$, in view of the dispersion $\omega_p(k)$ being relatively weak. We qualitatively estimate the transmission coefficient as the ratio of the band width for the electrons in the metal and free electrons: $D = m/m^*$. (We adopt $m^*/m = 1.28$ for the effective mass of the electron relative to its free-particle value.^{45,46}) Indeed, the band width scales with the tunneling matrix element, while one should recover $D = 1$ for free electrons. The factor 4 reflects that there are 4 inter-nuclear spaces separating closest neighbors in the BCC lattice per nucleus. This yields $x_{\text{liq}}/x_{\text{sol}} \approx 1.85$.

Thus we have argued that a substantial contribution to the overall electronic wavefunction is due to localized electrons. The photocurrent due to this contribution, per absorbed photon, is comparable to that stemming from the Fermi-liquid. Spectrally, the photocurrent due to localized sources is tied to the Fermi level, apart from some broadening. Put together, the above notions then rationalize the puzzling Fermi-energy photoemission peak in alkali metals. We evaluate the photoemission spectra for sodium, shown in Fig. 2, to be compared with Fig. 2 of Ref.¹. (Experimental spectra also contain a background due to a variety of processes,³⁶ not considered here.) The extent of broadening of the dispersive line was chosen by hand to be similar to that seen in the experiment; the breadth is nonetheless consistent with the electron's mean free path.⁴⁷⁻⁴⁹ The integrated intensity of the Fermi peak is less than that for the dispersive peak, when the latter is allowed, but the Fermi peak is also

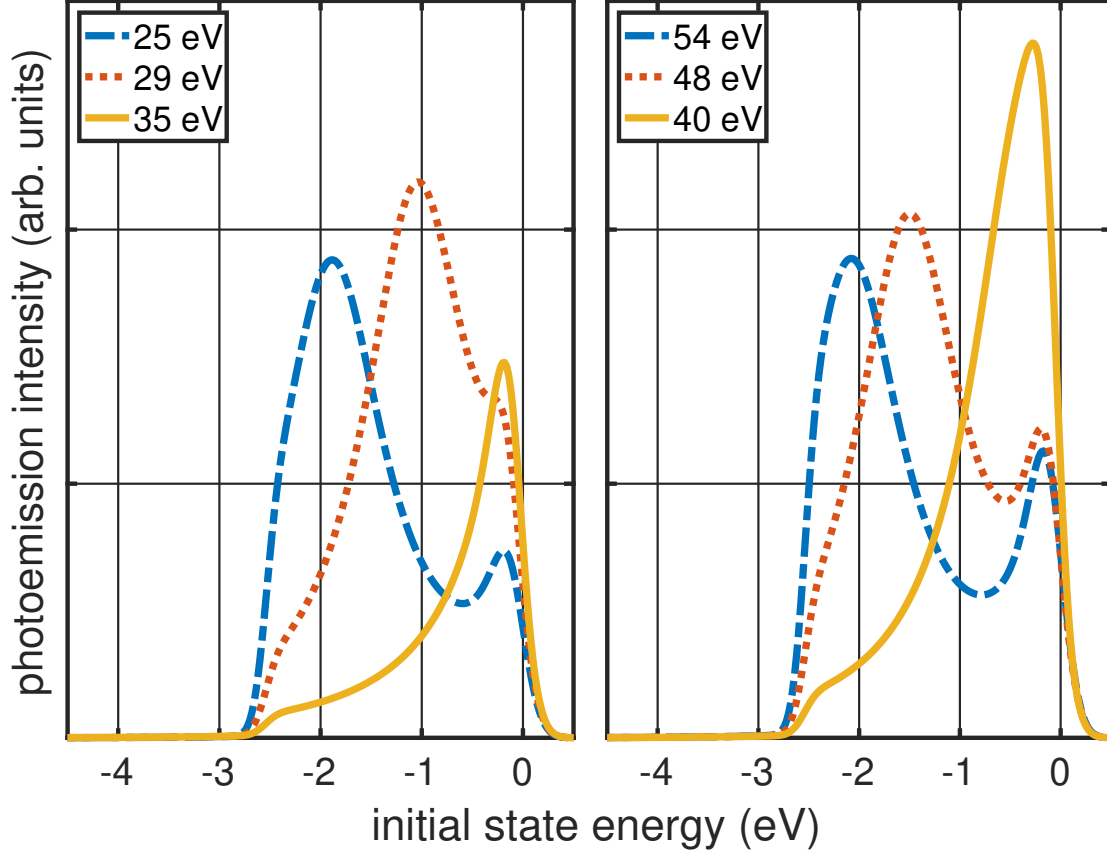


FIG. 2. Photoemission spectra from Eq. (2) data for sodium in the $(1,1,0)$ direction for select values of photon frequencies indicated in the legend, to be compared with Fig. 2 from Ref.¹. The electron energy is relative to the Fermi level. We set $\alpha = 1/2$ in Eq. (4).

sharper near the top and remains visible within a substantial range of photon energies. This is qualitatively consistent with experiment. Incidentally we note that the narrowness of the anomalous peak, relative to the dispersive peak, is consistent with the former stemming from non-itinerant electrons. Because the dispersive peak is broadened, its total intensity is somewhat diminished in the spectrally allowed range. Conversely, even when the center of the dispersive peak is in the spectrally forbidden region, its wings generally extend in the occupied region of the valence band, as in Refs.^{5,6}. The intensity ratio from Eq. (3) corrected for these broadening effects is shown in Fig. 1 with the dashed line. For the anomalous peak, we adopt the parametrization from Ref.⁵⁰.

To avoid ambiguity, we note the present analysis pertains exclusively to the bulk physics. Effects of the free surface are not included. Also, strictly speaking, on the short time scales

of photoemission, plasmons should be regarded as a symmetry lowering perturbation to the Fermi-liquid. These effects can be visualized and contribute to the background,^{32,51} see Supplemental Material.⁴⁰

Photoemission out of a localized state exhibits classical features, consonant with the infrared catastrophe²⁴ accompanying the recoil currents. (Similar catastrophes, leading to a classical-like localization of a quantum motion, take place as part of the Kondo-effect or, for instance, the localization of a particle interacting with a bath.⁵²) The photon's momentum and energy are initially imparted to the material within a localized region, before they are passed on to the rest of the electrons and the nuclei. The density of the grand-canonical free energy ($V = \text{const}$, $T = \text{const}$) is equal to the negative pressure.⁵³ Thus a photon impinging on a volume V effectively creates an excess negative pressure $-\hbar\omega_{\text{ph}}/V$, the corresponding forces being much greater than the characteristic electronic forces when $V \lesssim a^3(\hbar\omega/E_F) \simeq 10^1 a^3$. This negative pressure is, in fact, the driving force behind the decrease in local density caused by photoemission. This negative pressure will persist until the hole is filled by the recoil currents. When creating a localized hole, we are bringing in physical contact two distinct phases thus incurring a mismatch penalty. (If the interface is thin, the penalty amounts to a conventional surface tension.⁵³) Thus the formation of the hole is a *nucleation*-like process. Nucleation of a low-density phase caused by local excess of negative pressure is a well known phenomenon called “cavitation,” hence the title of the article. Nucleation, of course, is a strongly non-linear phenomenon; *homogeneous* nucleation furthermore represents a breaking of spatial symmetry.

As a dividend of the present analysis, we note that the metal acts as a transmitter of electrons, during photoemission, the final state of the particle being a plane wave. Conversely, one may consider the reciprocal process, in which the metal is the receiver. Hereby the electron is initially a plane wave and eventually enters the metal in the form of a localized object while filling a localized vacancy, whose concurrent formation is accompanied by recoil currents. This reciprocal process can be thought of as a detection event for the received electron, so that its location becomes known to the extent determined by the size and shape of the hole. As the measurement proceeds, the single-particle density matrix progressively deviates from its initial, nearly free-electron value. Thus the present scenario is an explicit example of how a measurement event is a result of a strongly non-linear, many-body phenomenon but can be profitably thought of as a “collapse” of a one-particle wavefunction,

if the full density-matrix of the system is unavailable. Because the event is an instance of symmetry breaking, its outcome is history dependent. This is analogous to how the precise magnetization pattern in a magnet below the Curie point or, to give another example, the detailed structure of a glass below the glass transition¹⁸ depend on the preparation protocol. Other, arguably simpler scenarios can be imagined. For example, consider a dilute gas or a set of deep core orbitals in a metal such that the photon's wavelength is much greater than the spatial separation between pertinent orbitals. An electron to be photoemitted is automatically localized within an orbital whose eventual identity will have emerged as a result of a symmetry lowering process and, thus, depends on the history. The non-linear phenomenon is whatever the process that causes individual orbitals not to form a band in the first place, such as a metal-insulator transition.⁵⁴ Likewise, receiving orbitals are also automatically localized.

Acknowledgments

We thank E. Ward Plummer (now deceased) and Gerry Mahan (now deceased) for inspiring conversations and Peter G. Wolynes and Eric Bittner for helpful insight. We gratefully acknowledge the support by the NSF Grants CHE-1465125 and CHE-1956389, the Welch Foundation Grant E-1765, and a grant from the Texas Center for Superconductivity at the University of Houston. We gratefully acknowledge the use of the Maxwell/Opuntia Cluster at the University of Houston. Partial support for this work was provided by resources of the uHPC cluster managed by the University of Houston and acquired through NSF Award Number ACI-1531814.

* Current address: Department of Electrical & Computer Engineering, Duke University, Durham, NC 27708

† vas@uh.edu

¹ E. Jensen and E. W. Plummer, Phys. Rev. Lett. **55**, 1912 (1985).

² B. S. Itchkawitz, I.-W. Lyo, and E. W. Plummer, Phys. Rev. B **41**, 8075 (1990).

³ E. W. Plummer, Physica Scripta **1987**, 186 (1987).

- ⁴ N. W. Ashcroft and N. D. Mermin, *Solid State Physics* (Harcourt Brace College Publishers, Fort Worth, 1976).
- ⁵ K. W. K. Shung and G. D. Mahan, Phys. Rev. Lett. **57**, 1076 (1986).
- ⁶ K. W. K. Shung, B. E. Sernelius, and G. D. Mahan, Phys. Rev. B **36**, 4499 (1987).
- ⁷ A. W. Overhauser, Phys. Rev. Lett. **58**, 959 (1987).
- ⁸ S.-K. Ma and K. W. K. Shung, Phys. Rev. B **50**, 5004 (1994).
- ⁹ A. W. Overhauser, Phys. Rev. Lett. **55**, 1916 (1985).
- ¹⁰ A. W. Overhauser, Adv. Phys. **27**, 343 (1978).
- ¹¹ D. Follstaedt and C. P. Slichter, Phys. Rev. B **13**, 1017 (1976).
- ¹² S. F. Elatresh, M. T. Hossain, T. Bhowmick, A. D. Grockowiak, W. Cai, W. A. Coniglio, S. W. Tozer, N. W. Ashcroft, S. A. Bonev, S. Deemyad, and R. Hoffmann, Phys. Rev. B **101**, 220103 (2020).
- ¹³ P. W. Anderson, *Basic Notions of Condensed Matter Physics* (Benjamin Cummins, Menlo Park, CA, 1984).
- ¹⁴ J. Goldstone and K. Gottfried, Il Nuovo Cimento (1955-1965) **13**, 849 (1959).
- ¹⁵ D. Pines, *Elementary Excitations in Solids* (W. A. Benjamin, New York, 1963).
- ¹⁶ P. Nozieres and D. Pines, *Theory Of Quantum Liquids*, Advanced Books Classics (Avalon Publishing, 1999).
- ¹⁷ L. D. Landau and E. M. Lifshitz, *Fluid Mechanics* (Pergamon Press, New York, 1987).
- ¹⁸ V. Lubchenko, Adv. Phys. **64**, 283 (2015).
- ¹⁹ J. Schmalian and P. G. Wolynes, Phys. Rev. Lett. **85**, 836 (2000).
- ²⁰ V. Lubchenko and P. G. Wolynes, Annu. Rev. Phys. Chem. **58**, 235 (2007).
- ²¹ B. Bernu, F. Delyon, L. Baguet, and M. Holzmann, Contributions to Plasma Physics **57**, 524 (2017).
- ²² J. R. Klauder and P. W. Anderson, Phys. Rev. **125**, 912 (1962).
- ²³ V. Lubchenko and R. J. Silbey, J. Chem. Phys. **126**, 064701 (2007).
- ²⁴ P. W. Anderson, Phys. Rev. Lett. **18**, 1049 (1967).
- ²⁵ L. Landau, Phys. Z. Sowjet. **11**, 26 (1937), English translation in "Collected Papers of Landau", 1965, Gordon and Breach.
- ²⁶ S. A. Brazovskii, JETP **41**, 85 (1975).
- ²⁷ M. G. Blaber, M. D. Arnold, and M. J. Ford, J. Phys. Chem. C **113**, 3041 (2009).

- ²⁸ P. Rabochiy and V. Lubchenko, J. Phys. Chem. B **116**, 5729 (2012).
- ²⁹ R. Feynman, *Statistical Mechanics: A Set Of Lectures*, Advanced Books Classics Series (Westview Press, Boulder, CO, 1998).
- ³⁰ J. C. Golden, V. Ho, and V. Lubchenko, J. Chem. Phys. **146**, 174502 (2017).
- ³¹ N. F. Mott, *Conduction in Non-crystalline Materials* (Clarendon Press, Oxford, 1993).
- ³² R. Dmitriev, *Transient Infrared Catastrophes in Correlated Electron Fluids and the Puzzles of Photoemission Spectra in Alkali Metals*, Ph.D. thesis, University of Houston (2021).
- ³³ N. Ashcroft, Physics Letters **23**, 48 (1966).
- ³⁴ K. W. K. Shung and G. D. Mahan, Phys. Rev. Lett. **57**, 1076 (1986).
- ³⁵ L. D. Landau and E. M. Lifshitz, *Quantum Mechanics* (Pergamon Press, 1981).
- ³⁶ S. Hüfner, *Photoelectron Spectroscopy: Principles and Applications*, Springer Series in Solid-State Sciences (Springer Berlin Heidelberg, 2013).
- ³⁷ C. Cohen-Tannoudji, B. Diu, and F. Laloe, *Quantum Mechanics, Volume 1* (Wiley, 1991).
- ³⁸ T. A. Albright, J. K. Burdett, and M.-H. Whangbo, *Orbital Interactions in Chemistry* (Wiley, Hoboken, NJ, 2013).
- ³⁹ N. Goldenfeld, *Lectures on phase transitions and the renormalization group* (Addison-Wesley, Reading, MA, 1992).
- ⁴⁰ See Supplemental Material at ...for the detailed derivation of the expressions for the photocurrent from Fermi-liquid-like and localized sources, as well as for illustration of the transient lowering of the crystal field, due to the plasmons.
- ⁴¹ S. Doniach and M. Sunjic, Journal of Physics C Solid State Physics **3**, 285 (1970).
- ⁴² J. Hopfield, Comments Solid State Phys. **2**, 40 (1969).
- ⁴³ J. Friedel, Adv. Phys. **3**, 446 (1954).
- ⁴⁴ P. Nozières and C. T. De Dominicis, Phys. Rev. **178**, 1097 (1969).
- ⁴⁵ W. H. Lien and N. E. Phillips, Phys. Rev. **118**, 958 (1960).
- ⁴⁶ C. C. Grimes and A. F. Kip, Phys. Rev. **132**, 1991 (1963).
- ⁴⁷ D. Gall, Journal of Applied Physics **119**, 085101 (2016), <https://doi.org/10.1063/1.4942216>.
- ⁴⁸ R. Kammerer, J. Barth, F. Gerken, C. Kunz, S. A. Flodstrøm, and L. I. Johansson, Phys. Rev. B **26**, 3491 (1982).
- ⁴⁹ Y. He and V. Lubchenko, J. Chem. Phys. **158**, 124119 (2023).
- ⁵⁰ G. D. Mahan, Phys. Rev. B **11**, 4814 (1975).

- ⁵¹ J. VandeVondele, M. Krack, F. Mohamed, M. Parrinello, T. Chassaing, and J. Hutter, *Comput. Phys. Commun.* **167**, 103 (2005).
- ⁵² A. J. Leggett, S. Chakravarty, A. T. Dorsey, M. P. A. Fisher, A. Garg, and W. Zwerger, *Rev. Mod. Phys.* **59**, 1 (1987).
- ⁵³ H. Y. Chan and V. Lubchenko, *J. Chem. Phys.* **143**, 124502 (2015).
- ⁵⁴ V. Lubchenko and A. Kurnosov, *J. Chem. Phys.* **150**, 244502 (2019).

Supplemental Material: Cavitation in Electron Fluids and the Puzzles of Photoemission Spectra in Alkali Metals

Roman Dmitriev¹, Jenny Green², and Vassiliy Lubchenko^{1,3,4}

¹Department of Chemistry, University of Houston, Houston, TX 77204-5003

²St. John's School, Houston, TX 77019

³Department of Physics, University of Houston, Houston, TX 77204-5005

⁴Texas Center for Superconductivity, University of Houston, Houston, TX 77204-5002

This Supplemental Material is organized as follows: In Section I, we detail the present estimates for the photocurrent due to both wavepacket-like and localized sources. In Section II, we illustrate effects of transient symmetry lowering due to plasma oscillations.

I. CALCULATION OF PHOTOCURRENT

We quantify the rate of photoemission using an effective one-particle description, whereby the initial state of the electron is described by an energy ε_i and wavefunction ψ_i , while in the final state, the electron's energy is ε_f and the wavefunction ψ_f . We evaluate the rate w_{fi} of transitions from the initial to the final electronic state, in the presence of a photon at frequency ω_{ph} , using the Fermi Golden rule:^{35,36}

$$w_{fi} = \frac{2\pi}{\hbar} |M_{f,i}|^2 \delta(\varepsilon_f - \varepsilon_i - \hbar\omega_{\text{ph}}), \quad (\text{S1})$$

where

$$M_{f,i} = \langle \psi_f | H' | \psi_i \rangle \quad (\text{S2})$$

is the one-particle transition matrix element for the perturbation H' due to the photon field. In the above expression, we have omitted the overlap of the rest $(N - 1)$ wavefunctions for the electrons that are left behind in the metal, following a photoemission event. This overlap generally differs from unity. The corresponding effects—along with those stemming from correlations—modify the line shape of the photoemission spectra, to be discussed in due time.

The photoemission spectrum $I(E, \hbar\omega_p)$ is the total current per unit of electron energy E :

$$I(E, \hbar\omega_{\text{ph}}) = \frac{2\pi}{\hbar} \sum_{i,f} |M_{f,i}|^2 \delta(\varepsilon_f - \varepsilon_i - \hbar\omega_{\text{ph}}) \delta(E - \varepsilon_f - \Phi), \quad (\text{S3})$$

where one sums over all possible initial and final states of the electron and the quantity Φ is the work function of the metal.

In angle-resolved photo-emission spectroscopy (ARPES), one determines the total amount of collected electrons per energy E and solid angle Ω . Hereby, one computes the photocurrent for electrons exiting the sample within a specified solid angle Ω_d :

$$I(E, \Omega, \hbar\omega_{\text{ph}}) = \frac{2\pi}{\hbar} \sum_{i,f} |M_{f,i}|^2 \delta(\varepsilon_f - \varepsilon_i - \hbar\omega_{\text{ph}}) \delta(E - \varepsilon_f - \Phi) \delta(\Omega - \Omega_d), \quad (\text{S4})$$

In the remainder of this Supplemental Material (SM), we will drop the multiplicative constant $2\pi/\hbar$, to declutter the formulas.

We limit ourselves to the common case of the outgoing electron's energy being much greater than the crystal field, so that the latter can be regarded as a weak perturbation. Thus we assume the electron's energy is a continuous quantity that obeys the dispersion relation for a free electron, as in Ref.¹:

$$\varepsilon_f(\mathbf{k}) = \hbar^2 k^2 / 2m. \quad (\text{S5})$$

Consequently, the summation over final states can be rewritten as a continuous integration over the wave vector of the outgoing electron:

$$I_\Omega(E, \Omega, \hbar\omega_{\text{ph}}) = \sum_i \int d^3\mathbf{k} |M_{f,i}|^2 \delta(\Omega(\mathbf{k}) - \Omega_d) \delta(\varepsilon_f(\mathbf{k}) - \varepsilon_i - \hbar\omega_{\text{ph}}) \delta(E - \varepsilon_f(\mathbf{k}) - \Phi) \quad (\text{S6})$$

We will suppose, in the conventional fashion, that the photoemitted electrons are collected in the direction normal to the surface of the sample; for instance in Jensen and Plummer's experiment,¹ this direction corresponds to the normal of the crystal plane (1, 1, 0). Thus we obtain

$$I_\Omega(E, \Omega, \hbar\omega_{\text{ph}}) = \sum_i \int dk k^2 |M_{f,i}|^2 \delta(\varepsilon_f(\mathbf{k}) - \varepsilon_i - \hbar\omega_{\text{ph}}) \delta(E - \varepsilon_f(\mathbf{k}) - \Phi) \quad (\text{S7})$$

Integration with respect to the momentum of the outgoing electron then yields

$$\begin{aligned} I(E, \hbar\omega_{\text{ph}}) &= \frac{k_f^2}{|d\varepsilon_f(k)/dk|_{k_f}} \sum_i |M_{f,i}|_{\mathbf{k}_f}^2 \delta(E - \varepsilon_f(\mathbf{k}_f) - \Phi) \\ &= \frac{m k_f}{\hbar^2} \sum_i |M_{f,i}|_{\mathbf{k}_f}^2 \delta(E - \varepsilon_f(\mathbf{k}_f) - \Phi) \end{aligned} \quad (\text{S8})$$

where the value of the outgoing momentum is fixed according to

$$\varepsilon_f(\mathbf{k}_f) - \varepsilon_i = \hbar\omega_{\text{ph}} \quad (\text{S9})$$

so as to satisfy energy conservation, as embodied by the first delta function in Eq. (S7).

To evaluate the transition matrix element we use the expression for the energy of an electron in the presence of electromagnetic field with the vector potential \mathbf{A} :³⁷

$$H = \frac{(\mathbf{p} - q_e \mathbf{A})^2}{2m} + U \equiv H_0 + H', \quad (\text{S10})$$

where q_e is the charge of the electron and H' is the perturbation due to the photon field, by construction. In the limit of linear response, one obtains:

$$H' = -\frac{q_e}{2m}(\mathbf{p}\mathbf{A} + \mathbf{A}\mathbf{p}) = -\frac{q_e}{m}\mathbf{A}\mathbf{p} = i\hbar\frac{q_e}{m}\mathbf{A}\nabla, \quad (\text{S11})$$

where we used $\mathbf{p} = -i\hbar\nabla$ and $\mathbf{p}\mathbf{A} = -i\hbar\nabla\mathbf{A} = -i\hbar[(\nabla \cdot \mathbf{A}) + \mathbf{A}\nabla] = -i\hbar\mathbf{A}\nabla = \mathbf{A}\mathbf{p}$, since in the Coulomb gauge $(\nabla \cdot \mathbf{A}) = 0$. Subsequently,

$$M_{f,i} \equiv \langle \psi_f | H' | \psi_i \rangle = -\frac{q_e}{m} \langle \psi_f | \mathbf{A}\mathbf{p} | \psi_i \rangle \quad (\text{S12})$$

where, specifically, the photon field is a plane wave

$$\mathbf{A} = \mathbf{e}A_0e^{i\mathbf{k}_{\text{ph}}\mathbf{r}}. \quad (\text{S13})$$

Here \mathbf{k}_{ph} denotes the photon's momentum and \mathbf{e} is the unit vector specifying the direction of the vector potential. Consequently, Eq. (S12) yields

$$|M_{f,i}|^2 = \left(\frac{q_e\hbar}{m}\right)^2 |\langle \psi_f(\mathbf{r}) | \mathbf{A}\nabla | \psi_i(\mathbf{r}) \rangle|^2 = \left(\frac{q_e\hbar}{m}\right)^2 |\langle \psi_i(\mathbf{r}) | \mathbf{A}^*\nabla | \psi_f(\mathbf{r}) \rangle|^2. \quad (\text{S14})$$

The final-state wavefunction is a plane wave, as already alluded to:

$$\psi_f(\mathbf{r}) = e^{i\mathbf{k}_f\mathbf{r}} \quad (\text{S15})$$

—where we do not need concern ourselves with the normalization—and so

$$\nabla\psi_f(\mathbf{r}) = i\mathbf{k}_f\psi_f(\mathbf{r}). \quad (\text{S16})$$

In what follows, we consider two cases: when the initial state is a Bloch wave and a localized entity, respectively.

A. Photocurrent due to Bloch states

We use the standard expression for a normalized Bloch wave:⁴

$$\begin{aligned}\psi_i(\mathbf{r}) &= \frac{1}{\sqrt{V}} \phi_{\mathbf{k}_i}(\mathbf{r}) e^{i\mathbf{k}_i \mathbf{r}} \\ \int_V d^3\mathbf{r} |\psi_i(\mathbf{r})|^2 &= 1\end{aligned}\tag{S17}$$

where the function $\phi_{\mathbf{k}_i}(\mathbf{r})$ has the periodicity of the crystal lattice and does not depend on the sample's size. Consequently, Eqs. (S14) and (S16) yield

$$|M_{f,i}|^2 = \frac{1}{V} \left(\frac{q_e A_0 \hbar}{m} \right)^2 \left| \int_V d^3\mathbf{r} e^{-i(\mathbf{k}_f - \mathbf{k}_i - \mathbf{k}_{\text{ph}})\mathbf{r}} \phi_{\mathbf{k}_i}(\mathbf{r}) \right|^2 (\mathbf{k}_f \mathbf{e})^2\tag{S18}$$

where we used Eqs. (S13) and (S15).

To make explicit the role of periodicity of the function $\phi_{\mathbf{k}_i}(\mathbf{r})$ —as stemming from the periodicity of the underlying crystal, of course—we present the Bloch state $\phi_{\mathbf{k}_i}(\mathbf{r})$ in Eq. (S18) as the following sum:

$$\phi_{\mathbf{k}_i}(\mathbf{r}) = \sum_j^N \phi^{(\text{loc})}(\mathbf{r} - \mathbf{r}_j, \mathbf{k}_i)\tag{S19}$$

where the points \mathbf{r}_j form a periodic array that mirrors the periodicity of the underlying crystal. It is convenient to think of space as broken up into cells, so that there is exactly one point \mathbf{r}_j per cell. The choice of the function $\phi^{(\text{loc})}$ is not unique, of course, and is made according to one's convenience. Any two functions $\phi^{(\text{loc})}(\mathbf{r} - \mathbf{r}_j, \mathbf{k}_i)$ pertaining to two distinct centers \mathbf{r}_j can overlap; for instance, a plane wave corresponds to $\phi(\mathbf{r} - \mathbf{r}_j, \mathbf{k}_i) = \text{const} = 1/N$. Still, we ordinarily have in mind such functions $\phi^{(\text{loc})}(\mathbf{r}, \mathbf{k}_i)$ whose magnitude rapidly decays away from the origin at sufficiently large distances, as would atomic wavefunctions. In any event, one may now present the integral over space in Eq. (S18), as a sum of integrals of individual functions $\phi^{(\text{loc})}(\mathbf{r}, \mathbf{k}_i)$:

$$|M_{f,i}|^2 = \frac{1}{V} \left(\frac{q_e A_0 \hbar}{m} \right)^2 \left| \sum_j e^{-i(\mathbf{k}_f - \mathbf{k}_i - \mathbf{k}_{\text{ph}})\mathbf{r}_j} \int d^3\mathbf{r} e^{-i(\mathbf{k}_f - \mathbf{k}_i - \mathbf{k}_{\text{ph}})(\mathbf{r} - \mathbf{r}_j)} \phi^{(\text{loc})}(\mathbf{r} - \mathbf{r}_j, \mathbf{k}_i) \right|^2 (\mathbf{k}_f \mathbf{e})^2.\tag{S20}$$

For a large system, the summation over the cells in Eq. (S20) singles out only such values of the vector $(\mathbf{k}_f - \mathbf{k}_i - \mathbf{k}_{\text{ph}})$ that are each equal to vectors of the reciprocal lattice, in which case the sum is equal to the number itself of the cells, i.e., V/v_c , where v_c is the cell's

volume. For all other values of that vector, the sum scales sub-thermodynamically, which then amounts to momentum conservation, up to Umklapp processes. One thus obtains:

$$|M_{f,i}|^2 = \frac{V}{v_c^2} \left(\frac{q_e A_0 \hbar}{m} \right)^2 (\mathbf{k}_f \mathbf{e})^2 \sum_{\mathbf{G}} \left| \tilde{\phi}^{(\text{loc})}(\mathbf{G}, \mathbf{k}_i) \right|^2 \delta_{\mathbf{k}_f - \mathbf{k}_i - \mathbf{k}_{\text{ph}}, \mathbf{G}} \quad (\text{S21})$$

$$\approx \frac{V}{v_c^2} \left(\frac{q_e A_0 \hbar}{m} \right)^2 (\mathbf{k}_f \mathbf{e})^2 \sum_{\mathbf{G}} \left| \tilde{\phi}^{(\text{loc})}(\mathbf{G}, \mathbf{k}_i) \right|^2 \delta_{\mathbf{k}_f - \mathbf{k}_i, \mathbf{G}} \quad (\text{S22})$$

where we define the Fourier transform of the function $\phi^{(\text{loc})}$ as follows:

$$\tilde{\phi}^{(\text{loc})}(\mathbf{q}, \mathbf{k}_i) = \int d^3 \mathbf{r} \phi^{(\text{loc})}(\mathbf{r}, \mathbf{k}_i) e^{-i \mathbf{q} \mathbf{r}} \quad (\text{S23})$$

The discrete sum in Eqs. (S21) and (S22) runs over all vectors \mathbf{G} of the lattice reciprocal to the lattice comprised by the cells. The approximate equality in Eq. (S22) holds as long as the photon's wave length is much greater than the unit cell—whereby $k_{\text{ph}} \ll G$ —which is the case at photon's energies in Plummer et al.'s studies.³ The delta-function in Eqs. (S21) and (S22) is of the Kronecker variety, so that summation over any of its arguments yields exactly *unity*, $\delta_{\mathbf{k}, \mathbf{k}} = 1$, while, at the same time, singling out the appropriate value of the argument in the rest of the expression. The set of the reciprocal vectors \mathbf{G} contains each vector exactly *once* and the summation over \mathbf{G} is already explicitly present in the expression. Consequently, if one must sum over any of the electronic momenta, this can be done via continuous integration using weight functions normalized to unity, not volume. Thus we explicitly see the amount of photocurrent scales linearly with the sample's volume, as it should. One may equivalently employ the Dirac delta-function instead of the Kronecker variety, using the conventional procedure explained, for instance, in Section 5.7.2 of Ref.³⁹: $V \delta_{\mathbf{k}_1, \mathbf{k}_2} \rightarrow (2\pi)^3 \delta(\mathbf{k}_1 - \mathbf{k}_2)$ while summation, if any, over electronic momenta must be replaced by continuous integration according to the prescription $\sum_{\mathbf{k}} \rightarrow V \int d^3 \mathbf{k} / (2\pi)^3$. The latter procedure however makes the thermodynamic scaling of the photocurrent less explicit.

Expression (S22) indicates that an electron to be photoejected must be a Bloch state, not a plane wave— $\phi_{\mathbf{k}_i}(\mathbf{r}) \neq \text{const}$ —in order for the integral over the cell to be non-vanishing; this is consistent with the general notion that a free electron can not absorb or emit a photon. To choose the appropriate approximation for the wavefunction that enters the rather general expression (S22), it is useful to survey the range of possible responses of the electron fluid in terms of the magnitude of the recoil momentum. We begin from the low-momentum limit, in which one formally assumes the molecular potential is only weakly non-uniform;

this appears to be the most common approximation.^{33,34} Hereby one focuses on the lowest order harmonics of the spatial variation the crystal field, which correspond to the spacing between nearest neighbors in the lattice. Using the following commutation relationship for the unperturbed single electron Hamiltonian H_0 :

$$[H_0, \mathbf{p}] = i\hbar \nabla U \quad (\text{S24})$$

we obtain:

$$i\hbar \langle \psi_f | \nabla U | \psi_i \rangle = \langle \psi_f | [H_0, \mathbf{p}] | \psi_i \rangle = (E_f - E_i) \langle \psi_f | \mathbf{p} | \psi_i \rangle, \quad (\text{S25})$$

where E_i and E_f are the pertinent eigenvalues of the unperturbed Hamiltonian H_0 . Eqs. (S12) and (S13) consequently yield that the transition matrix element is directly related to the corresponding matrix element of the force due to the crystal field:

$$M_{f,i} = -\frac{iq_e A_0 \hbar}{m(E_f - E_i)} \langle \psi_f | \mathbf{e} \nabla U | \psi_i \rangle = -\frac{iq_e A_0}{m\omega_{\text{ph}}} \langle \psi_f | \mathbf{e} \nabla U | \psi_i \rangle \quad (\text{S26})$$

and in the second equality we substituted $E_f - E_i = \hbar\omega_{\text{ph}}$, in view of Eq. (S3). Regarding the molecular potential as a perturbation, the lowest order approximation, in terms of ∇U , is obtained by setting $\phi_i(\mathbf{r}) = 1$. Repeating the steps leading to Eq. (S22), one thus obtains for the square of the transition moment, $|M_{f,i}|^2$, from Eq. (S4):

$$|M_{f,i}|^2 \approx V \left(\frac{q_e A_0 \hbar}{m} \right)^2 \sum_{\mathbf{G}} (\mathbf{e} \mathbf{G})^2 \frac{|\tilde{U}_{\mathbf{G}}|^2}{(\hbar\omega_{\text{ph}})^2} \delta_{\mathbf{k}_f - \mathbf{k}_i, \mathbf{G}} \quad (\text{S27})$$

where the quantity

$$\tilde{U}_{\mathbf{k}} \equiv \int_{\text{cell}} \frac{d^3 \mathbf{r}}{v_c} e^{-i\mathbf{k} \cdot \mathbf{r}} U(\mathbf{r}) \quad (\text{S28})$$

is the (discrete) Fourier component of the molecular field. Note the integration in Eq. (S28) is over the cell, not over the whole space, c.f. Eq. (S23).

In view of the long wavelength nature of the approximation leading to expression (S27), it seems difficult to ascertain the accuracy of the large- G terms in the sum over \mathbf{G} ; thus it seems prudent to include only the lowest- G term in the sum.

In contrast, the large \mathbf{k}_f asymptotics of the photocurrent are largely determined by the behavior of individual atomic wavefunctions near their respective nuclei. This is where the rate of spatial variation of the wave function reaches its maximum value, owing to the intense scattering of the electron off the largely unscreened potential due to the nucleus. To see this explicitly, we assume that in an alkali metal, only one frontier atomic orbital, call it $\psi_{\text{F}}(\mathbf{r})$,

contributes to the Bloch states. (This orbital, approximately, would be the 3s atomic orbital for Na or 4s orbital for K.) Hence, the following ansatz approximates the Bloch state of the initial state near the nuclei, the approximation being worse in the inter-nuclear space:³⁸

$$\psi_i(\mathbf{r}) = \frac{1}{\sqrt{N}} \sum_{\mathbf{R}} e^{i\mathbf{k}\mathbf{R}} \psi_{\text{fr}}(\mathbf{r} - \mathbf{R}) \quad (\text{S29})$$

where the summation is over the locations of the atomic cores. In view of Eqs. (S17) and (S19), the ansatz above implies $\phi^{(\text{loc})}(\mathbf{r}, \mathbf{k}_i) = v_c^{1/2} e^{-i\mathbf{k}_i\mathbf{r}} \psi_{\text{fr}}(\mathbf{r})$. Combined with momentum conservation, as expressed by the delta function in Eq. (S22), this yields:

$$\tilde{\phi}^{(\text{loc})}(\mathbf{G}, \mathbf{k}_i) \approx v_c^{1/2} \tilde{\psi}_{\text{fr}}(\mathbf{k}_f) \quad (\text{S30})$$

where we specifically adopt the primitive cell as the cell in Eq. (S21), so that $V/N = v_c$, and define the Fourier transform of the frontier orbital in the usual fashion:

$$\tilde{\psi}_{\text{fr}}(\mathbf{k}) = \int d^3\mathbf{r} e^{-i\mathbf{k}\mathbf{r}} \psi_{\text{fr}}(\mathbf{r}). \quad (\text{S31})$$

Thus the transition matrix element is approximately given by the Fourier transform of the frontier orbital at the momentum \mathbf{k}_f of the outgoing electron. The latter wavefunction has a singularity at the origin in the form of a discontinuity in the first derivative, due to scattering off the nucleus. Thus the leading large q asymptotics of the Fourier transform $\tilde{\psi}_{\text{fr}}(q)$ have the form of a power law decay. The magnitude of the tail is largely determined by the magnitude of the electron's wave function near the nucleus. Indeed, the atomic function in question corresponds to a vanishing orbital momentum, $l = 0$. Thus the radial portion of the wavefunction $\psi_{\text{fr}}(\mathbf{r})$ is given by a product of a relatively slow function, finite at the origin, that determines the nodal structure of the wavefunction and an exponentially decaying function that details the tunneling tail at large separations from the nucleus.³⁵ A straightforward calculation shows that the aforementioned power law tail, up to a factor of order one, is given by the expression

$$\tilde{\psi}_{\text{fr}}(q) \xrightarrow{q \rightarrow \infty} 4\pi \frac{\psi_{\text{fr}}(0)}{L q^4}. \quad (\text{S32})$$

where the quantity L reflects the gross rate of decay of the wavefunction away from the center. The expression above corresponds to the following, simplified form for the wavefunction near the nucleus: $\psi_{\text{fr}}(\mathbf{r}) \rightarrow \psi_{\text{fr}}(0) e^{-r/L}$.

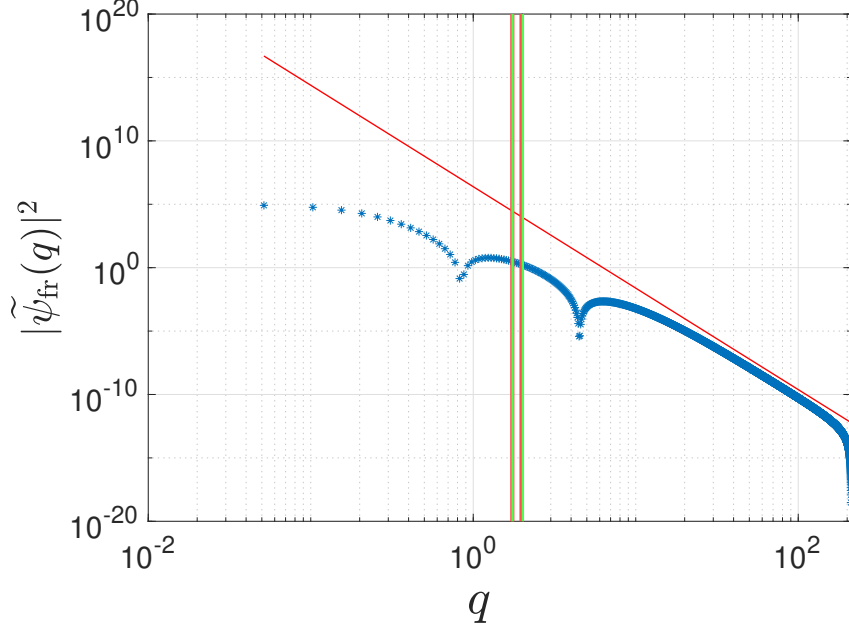


FIG. S1. Symbols: Square-modulus of the Fourier transform of the (numerically obtained) 3s Thomas-Fermi orbital of Na, as a function of the wavevector. The latter is given in atomic units. The thin solid red line indicates the slope of the power law dependence $1/q^8$. The two sets of vertical lines indicate the ranges of the momentum of the outgoing electron for the dispersive and non-dispersive peaks pertaining to Fig. 2 of the main text. The rapid decay on the r.h.s. of the q -range is due to the numerical error caused by the finite grid size.

In experiments of Plummer and coworkers, $k_f \sim 3k_F$. That is, the integral in Eq. (S30) probes spatial variations in the atomic function on length scales considerably less than the inter-atomic spacing but not quite in a regime where the large- q asymptotics from Eq. (S32) set in. We illustrate this by displaying the Fourier transform of the 3s Thomas-Fermi orbital for a standalone sodium atom in Fig. S1, where we indicate the ranges for the pertinent values of the momentum of the outgoing electron by sets of vertical lines. These pertinent values of momenta are separated by nodes from both the long-range and short-range behaviors of the wavefunction that are characteristic of the electronic motions, respectively, in the inter-nuclear space and near an unscreened nucleus. In the spirit of tight-binding approximations, we conclude that using the atomic function for ψ_{fr} may lead to a quantitative, but not qualitative error. Furthermore, this approximation will allow us to express the most important prediction of the present treatment, Eq. (3), in terms of a

ratio of quantities pertaining to the same object, which should mitigate the error, if any. In any event, we obtain for the matrix element, in view of Eq. (S21)

$$\begin{aligned} |M_{f,i}|^2 &\approx \frac{V}{v_c} \left(\frac{q_e A_0 \hbar}{m} \right)^2 (\mathbf{k}_f \mathbf{e})^2 \left| \int d^3 \mathbf{r} e^{-i \mathbf{k}_f \mathbf{r}} \psi_{\text{fr}}(\mathbf{r}) \right|^2 \sum_{\mathbf{G}} \delta_{\mathbf{k}_f - \mathbf{k}_i, \mathbf{G}} \\ &= \frac{V}{v_c} \left(\frac{q_e A_0 \hbar}{m} \right)^2 (\mathbf{k}_f \mathbf{e})^2 \left| \tilde{\psi}_{\text{fr}}(\mathbf{k}_f) \right|^2 \sum_{\mathbf{G}} \delta_{\mathbf{k}_f - \mathbf{k}_i, \mathbf{G}} \end{aligned} \quad (\text{S33})$$

In the assumption of the initial electronic state being a single-particle state, subject to a stationary crystal field, the contribution of each vector \mathbf{G} to the sums in Eqs. (S27) and (S33) is a sharp peak centered at energy $(\Phi + \varepsilon_i + \hbar \omega_{\text{ph}})$, per Eq. (S8). This notion, combined with the assumption on the dispersion of the outgoing electron, Eqs. (S5) and (S9), as well as momentum conservation, allows one to determine the one-particle spectrum $\varepsilon_i(\mathbf{k}_i)$ in the solid. In the presence of interactions, however, single-particle wavefunctions are no longer solutions of the Hamiltonian. As a result, the lifetime τ of a quasi-particle is intrinsically finite, which leads to a broadening of the photoemission line, in addition to the broadening due to factors than include, among others, lattice imperfections and finite spectral resolution of the spectrometer. In turn, this lifetime can be expressed through the mean free path l_{mfp} and the group velocity $\mathbf{v}(\mathbf{k}) = \partial \varepsilon / \partial (\hbar \mathbf{k})$ of the wavepacket:

$$\delta \varepsilon_i \approx \frac{\hbar}{\tau} \approx |\nabla_{\mathbf{k}} \varepsilon_i(\mathbf{k}_i)| \frac{1}{l_{\text{mfp}}}, \quad (\text{S34})$$

within a factor of order one.⁴⁹ The approximation underlying the simple result above can be discussed in a more formal vein: In the presence of many-body effects, single particle excitations are described using the (time-dependent) one-particle density matrix $\rho(\mathbf{r}_1, \mathbf{r}_2)$. One can Wigner transform this object: $\rho(\mathbf{r}, \mathbf{k}) = \int d^3(\mathbf{r}_2 - \mathbf{r}_1) \rho(\mathbf{r}_1, \mathbf{r}_2) e^{-i \mathbf{k}(\mathbf{r}_2 - \mathbf{r}_1)}$, take the limit of slow variation in terms of the center-of-mass variable $\mathbf{r} = (\mathbf{r}_1 + \mathbf{r}_2)/2$, and then Fourier transform in time. The resulting object, call it $\tilde{\rho}(\mathbf{k}, \omega)$, can be thought of as a distribution of the effective energy and momentum of the initial state of the quasiparticle. This distribution is maximized along a surface $\omega_0 = \omega_0(\mathbf{k}_0)$ in the four dimensional space formed by the three components of the wave-vector \mathbf{k} and the frequency $\omega = \varepsilon/\hbar$. The latter surface plays the role of the dispersion relation while the derivative $\partial \omega_0 / \partial \mathbf{k}_0$ corresponds with the group velocity of the quasiparticle, in the usual fashion. Momentum conservation in Eqs. (S21) and (S22) represents a rigid geometrical constraint, due to the periodicity, on which spatial harmonics of the (many-body) electronic wavefunction can contribute to

the photocurrent, see also Ref.⁷ Deviations from strict periodicity, if mild, can be effectively incorporated into the treatment by replacing the delta functions, in the momentum space, by sharply peaked functions of finite, small width. In any event, the energy of the initial state remains effectively distributed even if momentum is strictly conserved, the distribution given by $p(\omega) \propto \tilde{\rho}(\mathbf{k}, \omega)|_{\mathbf{k}=\mathbf{k}_f}$. The width of the energy distribution can be evaluated by multiplying the uncertainty in the momentum of the wavepacket $\delta p \equiv \hbar \delta k$ by the rate of dispersion in the direction of steepest descent $\nabla_{\mathbf{k}} \varepsilon = \nabla_{\mathbf{p}}(\mathbf{p}^2/2m^*) = \mathbf{p}/m^*$, the latter quantity being the group velocity itself, of course. The inverse of the wavevector uncertainty is simply the spatial extent $1/\delta k$ of the wavepacket, i.e., the mean free path; thus $\delta k \approx 1/l_{\text{mfp}}$. The corresponding uncertainty in the energy can be, then, approximately evaluated as follows:

$$\delta \varepsilon_i \approx |\nabla_{\mathbf{k}} \varepsilon_i(\mathbf{k}_i)| \delta k \approx |\nabla_{\mathbf{k}} \varepsilon_i(\mathbf{k}_i)| \frac{1}{l_{\text{mfp}}}, \quad (\text{S35})$$

as before. Already the simple parabolic dispersion relation works well in Na and K, in which the Fermi surface is spherical—to a very good approximation—and does not touch the boundaries of the Brillouin zone:

$$\varepsilon(\mathbf{k}_i) = \hbar^2 k_i^2 / 2m^* \quad (\text{S36})$$

where we dropped the subscript “0” for typographical clarity and m^* is the effective mass of the electron. Here we use $m^*/m = 1.28$, as in Ref.¹. This number happens to be close numerically to the midway value between the effective mass determined using calorimetry⁴⁵ and cyclotron resonance,⁴⁶ respectively.

Thus we conclude that for a given value of the momentum \mathbf{k}_i of the quasiparticle, the corresponding effective energy is distributed according to some (normalized) weight function $w_{\text{liq}}(\varepsilon_i - \varepsilon(\mathbf{k}_i), \delta \varepsilon_i)$:

$$\int dx w_{\text{liq}}(x, \delta \varepsilon_i) = 1, \quad (\text{S37})$$

In practical terms, the line-shape function w must replace the Dirac delta-function in Eq. (S8)—so as to phenomenologically account for interactions—where the quantity $\delta \varepsilon_i$ denotes the characteristic width of the broadened spectrum. Finally, the label “liq” in Eq. (S37) refers to the fact that we are describing the liquid-like portion of the response of the electron assembly. Here we will use the Lorentzian as the line shape:

$$w_{\text{liq}}(x) = \frac{\Gamma/\pi}{x^2 + \Gamma^2} \quad (\text{S38})$$

thus neglecting the frequency dependence, if any, of the imaginary part of the electron's self energy. In this work, we set $\Gamma = 0.6$ eV. This corresponds to $l_{\text{mfp}} \approx 9\text{\AA}$ by Eq. (S35) near k_F .

After putting together the above notions, we obtain for the photocurrent due to the Fermi-liquid component of the overall electronic response:

$$I_{\text{liq}}(E, \hbar\omega_{\text{ph}}) = 2 \frac{V}{v_c} \frac{k_f(q_e A_0)^2}{m} (\mathbf{k}_f \mathbf{e})^2 \left| \tilde{\psi}_{\text{fr}}(\mathbf{k}_f) \right|^2 \\ \times w_{\text{liq}}(E - \varepsilon_f(\mathbf{k}_f) - \Phi), \delta\varepsilon_i) \theta((\Phi + E_F + \hbar\omega_{\text{ph}}) - E) \times \theta(E - (\Phi + \hbar\omega_{\text{ph}})) \quad (\text{S39})$$

where the value of \mathbf{k}_f is fixed by energy conservation per Eq. (S9), combined with the constraint that $\mathbf{k}_f - \mathbf{k}_i = \mathbf{G}$, and by the location of the detector. A summation over all possible values of the reciprocal lattice vector \mathbf{G} is implied. In practice, there will be ordinarily just one such vector, if any. The multiplicative factor of 2 in the front has appeared because we have explicitly summed over the electron spin.

Finally, the step functions θ are included in Eq. (S39) to explicitly enforce that the effective energy of the initial state be contained within the occupied portion of the pertinent band. (We place the bottom of the band at $\varepsilon = 0$, per Eq. (S36).) Note the first step function should be replaced by the Fermi distribution at finite temperatures. In any event, because $\delta\varepsilon_i > 0$, the line-shape envelope w_{liq} will generally extend outside the occupied portion of the band, even if centered on an occupied orbital. Thus the overall contribution of the electron liquid to the photocurrent—as integrated over the *occupied* orbitals—will be less than when $\delta\varepsilon_i = 0$. The decrease will be the more significant, the closer the nominal peak's maximum $\varepsilon_i(\mathbf{k}_i)$ is to the edges of the occupied part of the band and, in particular, to the Fermi energy. Conversely, some photocurrent will be observed that corresponds to wings of spectral lines centered at nominally empty orbitals, $\varepsilon_i(\mathbf{k}_i) > E_F$ and $\varepsilon_i(\mathbf{k}_i) < 0$.

B. Photocurrent due to localized sources, and its value relative to the contribution of the Bloch states

When the initial state is localized in space, one must compute the transition matrix element for an individual initial state and then sum over the latter states to obtain the total photocurrent due to this mechanism. Using the general expression (S14), one readily obtains

that the photocurrent due to an individual localized orbital can be expressed through the Fourier transform of the orbital at $\mathbf{k} = \mathbf{k}_f$:

$$|M_{f,i}|^2 = \left(\frac{q_e A_0 \hbar}{m} \right)^2 (\mathbf{k}_f \mathbf{e})^2 \left| \int d^3 \mathbf{r} e^{-i \mathbf{k}_f \mathbf{r}} \psi_i^{(\text{loc})}(\mathbf{r}) \right|^2 \quad (\text{S40})$$

and we have indicated that the summation over the initial states is now a discrete sum over distinct localized sources of photocurrent.

As discussed in the main text, the effective energy of a localized state is distributed around the Fermi energy: $\varepsilon_i \approx E_F$. The broadening is due to the states being short-lived and due to the recoil of the Fermi-liquid. We denote this distribution with function $w_{\text{sol}}(x)$:

$$\int dx w_{\text{sol}}(x) = 1, \quad (\text{S41})$$

Here we make the simplest assumption of the spectral shape above being uncorrelated from the location in space or detailed shape of the respective wave function. Thus the solid-like contribution of the photocurrent is given by the expression

$$I_{\text{sol}}(E, \hbar\omega_{\text{ph}}) = \frac{V}{v_c} \frac{k_f (q_e A_0)^2}{m} n_l (\mathbf{k}_f \mathbf{e})^2 \left\langle \left| \tilde{\psi}_{\text{loc}}(\mathbf{k}_f) \right|^2 \right\rangle w_{\text{sol}}(E - (\Phi + E_F + \hbar\omega_{\text{ph}})) \quad (\text{S42})$$

where n_l is the number of localized sources per cell and the averaging is over distinct shapes of the effective wavefunction $\psi_{\text{loc}}(\mathbf{r})$. Note that values of the momentum of the outgoing electron for the delocalized and localized sources of photocurrent are generally different, at the same value of the photon frequency. The difference is, however, not very large because $\hbar\omega_{\text{ph}} \gg E_F$.

In contrast with the Fermi liquid case, the spectral broadening encoded by the function w_{sol} in Eq. (S42) does not lead to a decrease in the total amount of the corresponding photocurrent since, by construction, we consider occupied states only. Incidentally, the broadening due to the recoil currents is exclusively toward the occupied side of the Fermi energy, $\varepsilon_i \leq E_F$, in the first place. We use Eq. (2.7) from Mahan's article,⁵⁰ in which we set $g = 0.5$ and $\epsilon_0 = 0.85$ eV. This form exhibits the requisite low-energy asymptotics while being integrable. Additionally, we convolute this form with a Gaussian with standard deviation 0.15 eV to phenomenologically account for the spectral-diffusion broadening, discussed in the main text, as well as the finite resolution of the detector.

To compare the contribution of the localized sources of photocurrent to that of the extended ones, we adopt a specific functional form for the wavefunction of the initial states. As

explained in the main text, an appropriate functional form is represented by the Gaussian function:

$$\psi_{\text{loc}}(\mathbf{r}) = \psi_q(\mathbf{r}) \equiv (q^2/\pi)^{3/4} e^{-q^2 r^2/2} \quad (\text{S43})$$

and so,

$$\left\langle \left| \tilde{\psi}_{\text{loc}}(\mathbf{k}_f) \right|^2 \right\rangle = \left\langle \frac{8\pi^{3/2}}{q^3} e^{-k_f^2/q^2} \right\rangle_q, \quad (\text{S44})$$

while the averaging is now with respect to the parameter q . The expression in the angular brackets effectively describes the dependence of the amount of recoil from the localized charge proper on the degree of localization. Judging from the sigmodal dependence of the exponential on the r.h.s, we see the recoil is dominated by configurations of the electron fluid such that $q \gtrsim k_f$. We quantify this large- q response by performing the averaging above using the probability density of the frontier orbital, in the momentum space, as discussed in the main text. This probability density is simply the magnitude squared of the Fourier transform of the frontier wavefunction, normalized to unity. Given the definition (S31), the normalization factor is $(2\pi)^{-3}$ yielding for the effective probability distribution

$$p(q) = 4\pi q^2 \left| \tilde{\psi}_{\text{fr}}(q) \right|^2 / (2\pi)^3. \quad (\text{S45})$$

and, consequently:

$$\left\langle \left| \tilde{\psi}_{\text{loc}}(\mathbf{k}_f) \right|^2 \right\rangle = \frac{4}{\pi^{1/2}} \int_0^\infty \frac{dq}{q} e^{-k_f^2/q^2} \left| \tilde{\psi}_{\text{fr}}(q) \right|^2 \quad (\text{S46})$$

Finally, we obtain for the photocurrent:

$$I_{\text{sol}}(E, \hbar\omega_{\text{ph}}) = \frac{4}{\pi^{1/2}} \frac{V}{v_c} \frac{k_f(q_e A_0)^2}{m} (\mathbf{k}_f \mathbf{e})^2 \int_0^\infty \frac{dq}{q} e^{-k_f^2/q^2} \left| \tilde{\psi}_{\text{fr}}(q) \right|^2 \times w_{\text{sol}}(E - (\Phi + E_F + \hbar\omega_{\text{ph}})) \quad (\text{S47})$$

where the value of \mathbf{k}_f is fixed by energy conservation:

$$\varepsilon_f(\mathbf{k}_f) - E_F = \hbar\omega_{\text{ph}} \quad (\text{S48})$$

and we adopt the primitive cell as our repeat unit; thus $n_l = 1$.

Aside from the aforementioned complications due to line broadening accompanying the liquid response, the ratio of the cumulative intensities of the liquid-like and solid-like responses, respectively, reduces to a rather simple expression, according to Eqs. (S39) and (S47):

$$\frac{I_{\text{liq}}}{I_{\text{sol}}} = \frac{\pi^{1/2}}{2} \frac{k_{f,\text{liq}}^3}{k_{f,\text{sol}}^3} \frac{\left| \tilde{\psi}_{\text{fr}}(k_{f,\text{liq}}) \right|^2}{\int_0^\infty \frac{dq}{q} e^{-k_{f,\text{sol}}^2/q^2} \left| \tilde{\psi}_{\text{fr}}(q) \right|^2} \quad (\text{S49})$$

This expression is given as Eq. (3) of the main text. We see the solid response is an integral measure of the electronic wavefunction and, thus, is less sensitive to its detailed form than its liquid counterpart. The actual contributions of the liquid- and solid-like types of response will also depend on the relative amount of time the electron spends in the classically forbidden and allowed regions, respectively, as discussed in the main text. In addition, the details of line broadening will also affect the appearance of the spectra. While we expect the liquid-like response to yield an approximately Lorentzian shape, the contribution of the photocurrent due to the localized states has a more complicated functional form. The respective peak will be relatively narrow near the maximum but will also have a much broader base, because of the power-law spectrum of the recoil currents. This will act to make the peak's maximum more prominent.

II. PLASMA OSCILLATIONS AS A SYMMETRY-LOWERING PERTURBATION OF THE FERMI-LIQUID STATE

Plasma oscillations are considerably faster than the motions of valence electrons, and so, by construction, we regard the quasi-equilibrium, Fermi-liquid response of the electron fluid as effectively averaged over all instantaneous configurations of the plasmons. Furthermore, on these long time scales, the electronic excitations can be thought of as relatively well defined quasiparticles that are decoupled from the plasmons and whose mutual interaction is screened owing to the plasma oscillations.^{15,16}

On timescales of photoemission, however, plasmons are largely static objects that lower the symmetry of the molecular field. One may inquire how the Fermi-liquid part of the electronic response is affected by this circumstance. An upper bound for the effects of the aforementioned symmetry lowering can be obtained by assuming the electrons can instantly adjust to the plasmon configuration. Under these circumstances, the plasmon simply plays the role of an externally imposed static potential, analogously to how in the Born-Oppenheimer approximation, we regard the field due to nuclei as static. This construct can be also usefully looked at from the viewpoint of the density-functional theory. Suppose we can solve the electronic problem with an added source field. We can then perform a Legendre transform so as to obtain the energy of the system as a function of the spatial profile of the electron density.³⁰

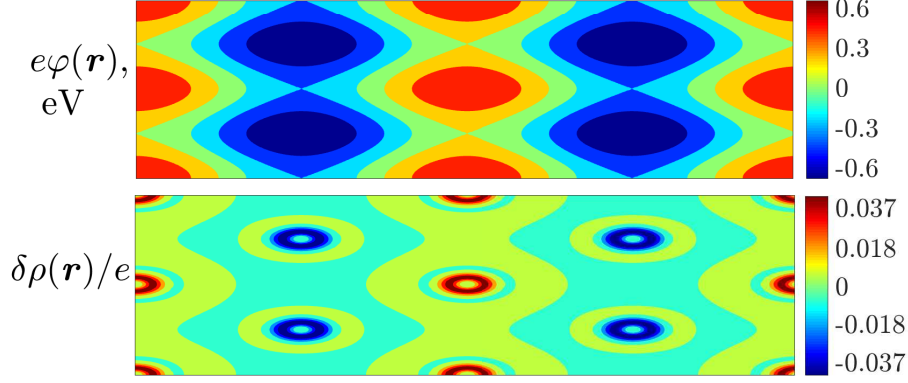


FIG. S2. Examples of externally applied field $\varphi(\mathbf{r})$ and the resulting deviation $\delta\rho$ of charge density from its $\varphi = 0$ value in potassium, slice along $(1, 1, 0)$. The magnitude of the potential 1.29 eV corresponds to the onset of the Van Hove singularity.

Here we specifically consider a perturbation that lowers the symmetry of the BCC structure found in Na and K, to that of the CsCl structure. The latter can be thought of as two inter-penetrating cubic lattices, one made of element A and the other of element B, where each corner of the A lattice is in the center of the cubic cell of lattice B and vice versa. We use the package CP2K⁵¹ to implement this construct. Fig. S2(a) shows the spatial profile of the perturbing potential, while the Fig. S2(b) shows the resulting change in the electron density.

One can directly observe that the perturbation illustrated in Fig. S2 leads to a distortion of the Fermi surface. For fields greater than a certain threshold value, the Fermi surface intersects the boundary of the Brillouin zone and is no longer simply connected while there appears a Van Hove singularity, see Fig. S3. If present in a static spectrum, such a singularity would give rise to a sharp feature for a vertical transition starting from the stationary point on the spectrum. If off resonance, the feature would still persist—if spectral line is broadened—but its integrated intensity would be scaled down by magnitude of the line-shape profile at the energy corresponding to the Van Hove singularity. In addition, the singularity is tied to the edge of the Brillouin zone (of the CsCl structure) in terms of the momentum but not in terms of energy, which will further smear contributions of peak due to individual charge-density configurations.

To quantify this upper bound on these non-adiabatic effects on the Fermi-liquid, one needs to average over all configurations of the fluid, such as that in Fig. S2(b), subject to the

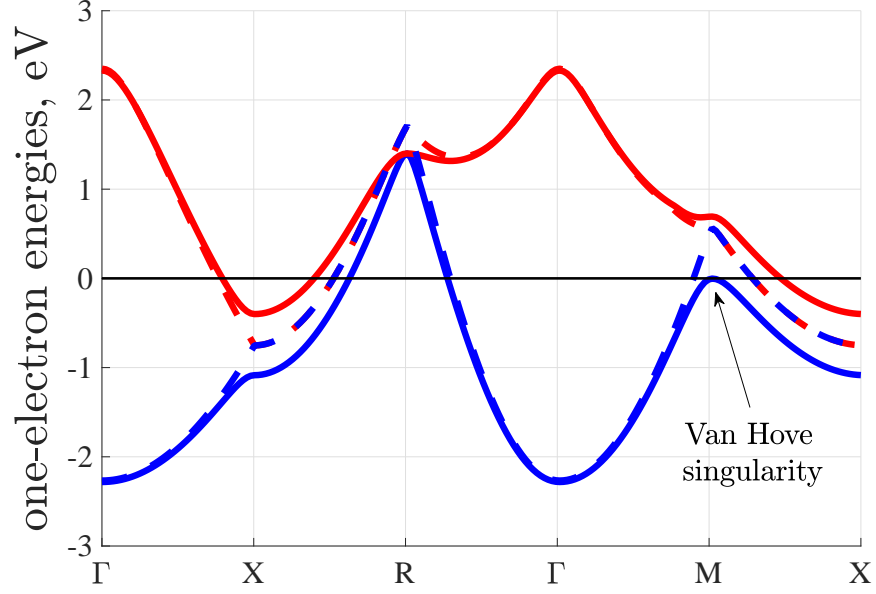


FIG. S3. The one-electron spectrum of elemental K with and without externally imposed potential shown, respectively, by the solid and dashed lines. The magnitude of the potential is 1.29 eV.

aforementioned density functional. We have performed such a calculation using a particular realization of the molecular field of the correct symmetry³² and the specific symmetry of the perturbing field from Fig. S2. We have found that the overall effect of the Van Hove singularities is modest overall and contributes to the background in the spectra but does not engender sharp features. This finding is consistent with the notion, stated in the main text, that the anomalous Fermi peak is a non-perturbative effect.